Supporting information

Interlayer-release synthesis of Cu single atoms anchored on heterogeneous photocatalyst for constructing Cu-Ov-Fe bimetallic active sites with ultrafast activation kinetics of H_2O_2

Changdong Chen[a,c], Yan Shang[a], Shihui Shao[a], Wei Wang[b], Jiahao Zhu[a], Ying Gao[a], Lei Chen[a], Fangfang Wang[a,]*

AUTHOR ADDRESS.

[a]School of petrochemical Engineering, Liaoning Petrochemical University, Fushun 113001, Liaoning, China.

[b]*College of Chemistry and Chemical Engineering, Jinggangshan University, Ji′an 343009, Jiangxi, China.*

[c]Department of Advanced Materials Science, Faculty of Engineering, Kagawa University, Takamatsu, 761-0396, Japan.

*Corresponding Authors: fionawang@xmu.edu.cn (Fangfang Wang)

Experimental details

1. characterization

The crystalline structures of the prepared catalysts were analyzed on a Bruker D8 Advance X-ray diffraction. The morphology, energy-dispersive X-ray spectroscopy mapping, and interface properties of the heterojunctions were performed on Hitachi SU8010 SEM and JEOL JEM- 2100F HR-TEM at 200 kV. AC-HAADF-STEM analysis was conducted on FEI Theims Z STEM system. Steady-state photoluminescence (SS-PL) spectra and time-resolved PL (TR-PL) were acquired from Edinburgh FLS1000 fluorescence spectrometer. In-Situ-X-ray photoelectron spectroscopy were performed on Thermofisher ESCALAB 250Xi XPS system. Electron spin resonance (ESR) spectra were recorded on Bruker EMX PLUS with 5,5-dimethyl-1-pyrroline N-oxide (DMPO) used as the spin trapping agent. Raman spectra of the samples were recorded on Thermo Fisher DXR Raman instrument with a 532 nm laser. NH_3 Temperature Programmed Desorption (NH_3-TPD) were investigated on Chembet Pulsar chemisorption analyzer. BET specific surface area analysis were conducted on Autosorb-IQ2-MP.

2. Catalytic activity test

In brief, 50 mg catalyst was added to a 100 mL solution of Phenol (20ppm) and sonicated for 5 minutes to disperse it evenly. After stirring vigorously for 30 minutes to reach adsorption/desorption equilibrium, the prepared suspension was injected with 0.15 mL H_2O_2 to initiate the reaction under Xe lamp illumination. 4mL of the reaction solution was collected at predetermined time intervals, and centrifuged for catalyst removal. To quench the ROSs, 0.5mL of methanol was added immediately into the collected solutions. The residual phenol was quantified using gas chromatography (Agilent 7890A) equipped with a PEG-20M column, and N_2 as carrier gas. The initial pH value of the reaction solution should be adjusted using H_2SO_4 or NaOH (0.5 mol/L) in order to investigate the impact of pH on Fenton-like catalytic process. The

used catalysts were centrifuged, rinsed with deionized water and dried at 60 °C in a vacuum oven for further evaluation of the catalyst's cyclic stability and durability.

3. Cyclic stability and durability test

Multiple parallel reactions were conducted simultaneously in each testing cycle to ensure sufficient samples could be recycled for the next round of testing. After each testing cycle, the catalyst powder was separated from the solution by centrifugation, washed with deionized water and ethanol for five times, and dried at 60 °C under vacuum overnight.

4. Photoelectrochemical Measurement

Electrode Preparation: 1 mg of catalyst was ultrasonically dispersed in 500 uL ethanol. Subsequently, a solution of Nafion (50uL) was added to the suspension and sonicated for 30 minutes to ensure uniform dispersion. Then 30 uL of the suspension was dripped on the FTO glass (1cm×1cm) and dried in ambient condition. This process was repeated three times, and the resulting FTO coated with sample film was left to dry overnight.

Photoelectrochemical (PEC) measurements: PEC measurements were conducted using a CHI660e electrochemical workstation. The electrolyte was a degassed 0.5 M Na_2SO_4 solution, which was treated with high-purity N_2 for 30 minutes to remove any dissolved gases. However, for the electrochemical impedance spectroscopy (EIS), the experiment was performed in a 0.1 M KCl solution containing 5 mM $K_3[Fe(CN)_6]/K_4[Fe(CN)_6]$ (1：1) at open circuit potential.

5. Calculation methods and details

The spin-polarized DFT calculations were performed using the VASP software based on the plane-wave basis sets with the projector augmented-wave method. The exchange-correlation potential was treated with a generalized gradient approximation (GGA) with the Perdew-Burke-Ernzerhof (PBE) parametrization. A vacuum region of about 15 Å was used to avoid the interaction between adjacent images. An energy cutoff of 450 eV was used. The Brillouin-zone integration was sampled with a Γ-

centered Monkhorst-Pack mesh of 3 × 3 × 1. The structures were fully relaxed until the maximum force on each atom was less than 0.05 eV/Å, and the energy convergent standard was set at 10^{-5} eV.

Results:

Table S1 Content of elements of Cu-O_v-Fe_2O_3/$CuFeO_2$ based on XPS analysis results

Elements	*Fe*	*O*	*Cu*
Contents (wt%)	58.7	26.5	14.8

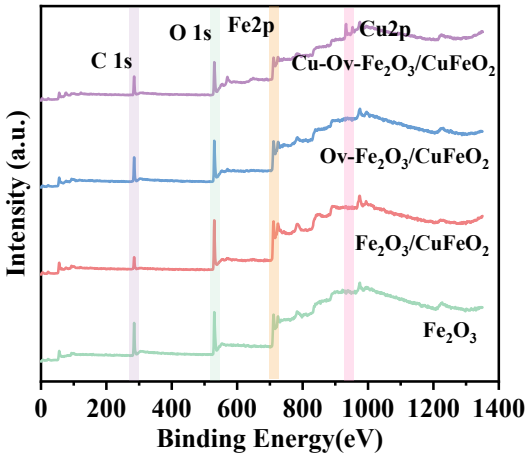

Fig. S1 XPS spectra of Cu-O_v-Fe_2O_3/$CuFeO_2$, O_v-Fe_2O_3/$CuFeO_2$, Fe_2O_3/$CuFeO_2$ and Fe_2O_3

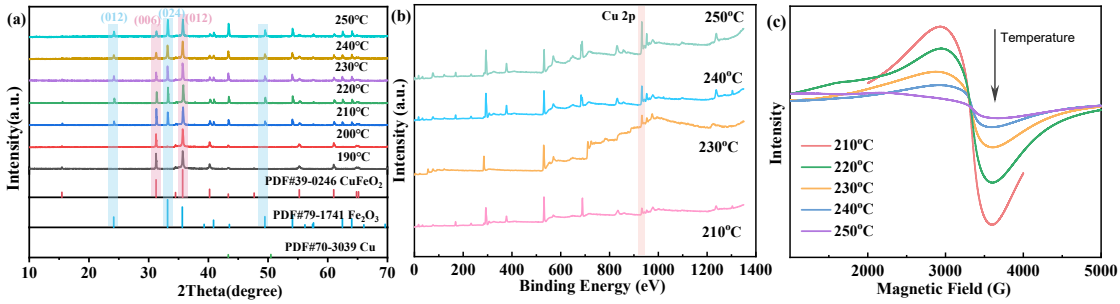

Fig.S2 (a)XRD patterns, (b) EPR Spectra of x%Cu-O_v-Fe_2O_3/$CuFeO_2$ prepared in different reaction temperatures.

The content of Fe_2O_3 and Cu gradually increases with increasing temperature, while the content of Ov decreases.

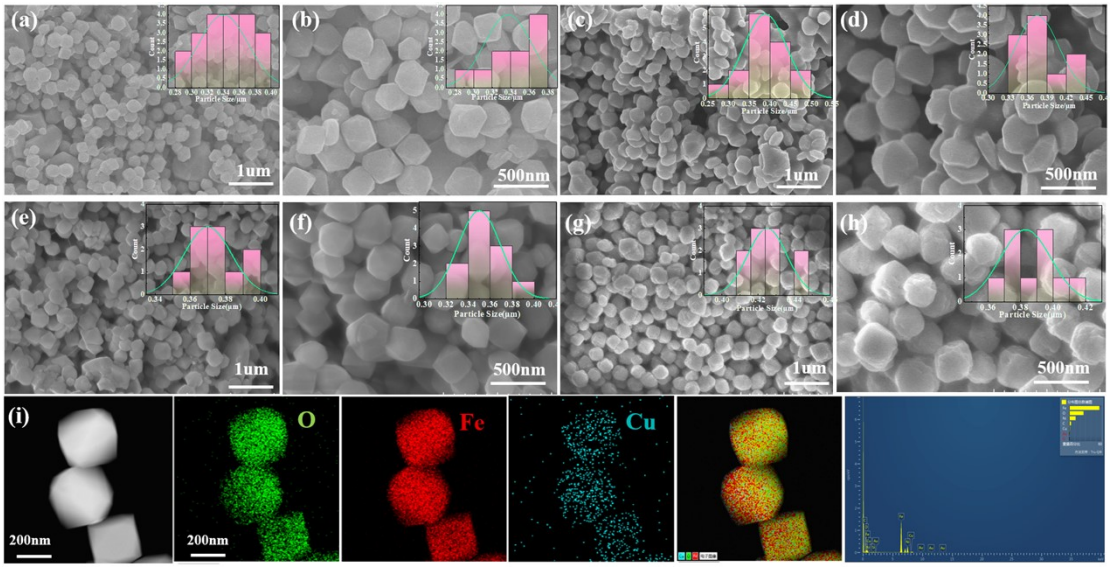

Fig.S3 SEM of (a,b) Cu-O_v-Fe_2O_3/$CuFeO_2$, (c,d) O_v-Fe_2O_3/$CuFeO_2$, (e,f) Fe_2O_3/$CuFeO_2$, (g,h) Fe_2O_3, (i) elemental mapping images of O, Fe Cu, and their overlapped images of Cu-O_v-Fe_2O_3/$CuFeO_2$.

Table S2 Fitting parameters of TRPL of Cu-O_v-Fe_2O_3/$CuFeO_2$, O_v-Fe_2O_3/$CuFeO_2$, Fe_2O_3/$CuFeO_2$, Fe_2O_3

Samples	B_1	τ_1	B_2	τ_2	τ_{ave}
Cu-O_v-Fe_2O_3/$CuFeO_2$	55.51	2.88	55.51	3.52	3.23
O_v-Fe_2O_3/$CuFeO_2$	8.16	5.04	8.16	6.16	5.66
Fe_2O_3/$CuFeO_2$	16.87	3.97	16.87	4.85	4.45
Fe_2O_3	21.65	3.69	21.65	4.51	4.14

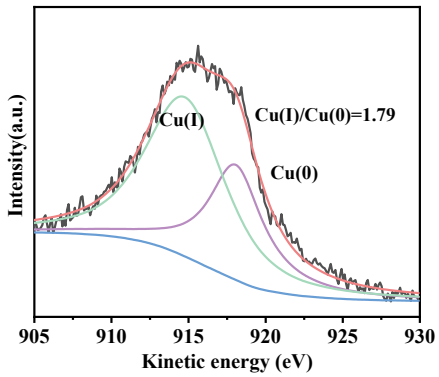

Fig.S4 Cu LMM Spectrum of Cu-O_v-Fe_2O_3/$CuFeO_2$ after turn off the light.

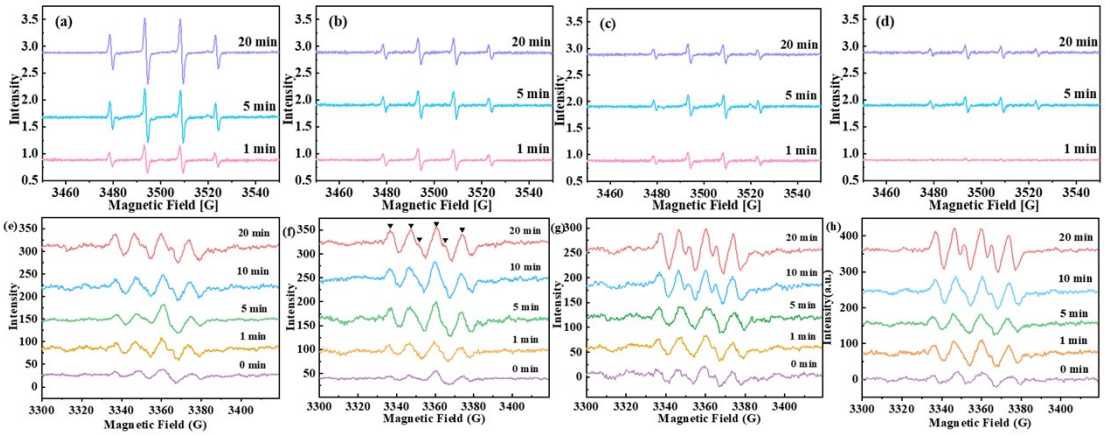

Fig.S5 (a-d) Time resolved ESR spectra of DMPO-•OH in different catalyst-H_2O_2 systems. (e-h) Time resolved ESR spectra of DMPO-•O_2^- in different catalyst-H_2O_2 systems.

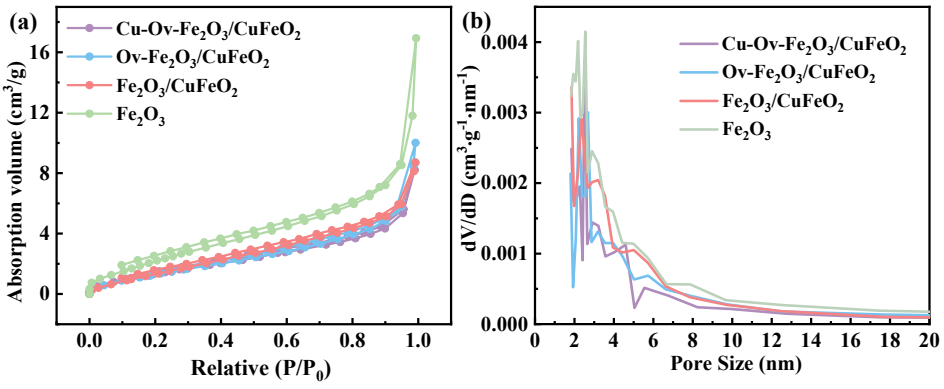

Fig. S6 BET measurements on Cu-O_v-Fe_2O_3/$CuFeO_2$, O_v-Fe_2O_3/$CuFeO_2$, Fe_2O_3/$CuFeO_2$ and Fe_2O_3: (a) N_2 adsorption-desorption isotherms, and (b) pore size distribution curves.

Table S3 Summary of textural properties of the samples

Samples	Specific Surface Area (m^2/g)	Pore Volume (cm^3/g)	Average Pore Size (nm)
Cu-Ov-Fe_2O_3/$CuFeO_2$	6.05	0.01	6.53
Ov-Fe_2O_3/$CuFeO_2$	5.34	0.01	7.16
Fe_2O_3/$CuFeO_2$	7.38	0.01	5.65
Fe_2O_3	10.13	0.02	7.11

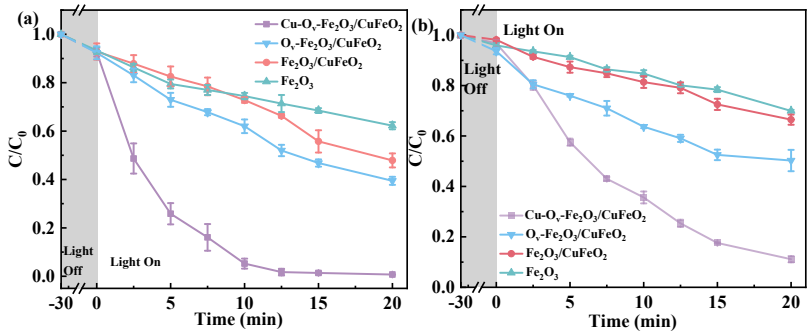

Fig.S7 Degradation of (a) tetracycline and (b)ciprofloxacin in Cu-O_v-Fe_2O_3/$CuFeO_2$, O_v-Fe_2O_3/$CuFeO_2$, Fe_2O_3/$CuFeO_2$ and Fe_2O_3 reaction systems.

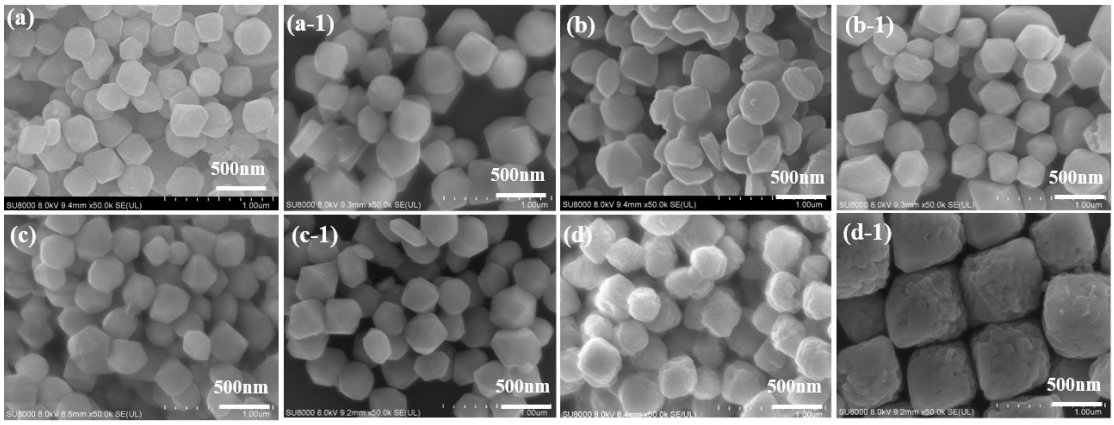

Fig.S8 Comparative analysis of morphological changes before and after the recycling experiment conducted on the prepared samples: (a, a-1) Cu-Ov-Fe_2O_3/$CuFeO_2$; (b, b-1) Ov-Fe_2O_3/$CuFeO_2$; (c, c-1) Fe_2O_3/$CuFeO_2$; (d, d-1) Fe_2O_3.

Table S4 Comparisons of heterogeneous Fenton-like catalysts for H_2O_2 activation.

Catalysts (g/L)	[pollutants] (mg/L)	[H_2O_2] (mM/L)	k_{obs} (min^{-1})	K-Value ($min^{-1}\cdot M^{-1}$)	Ref.
Cu-Ov-Fe_2O_3/CFO (0.5)	Phenol (20)	15	0.273	0.729	This Work
Cu/NC-MMT (0.5)	Phenol (20)	23.48	0.121	0.206	[1]
Cu_5/FeS_2 (0.5)	Alachlor (10)	0.8	0.236	5.9	[2]
CoFe2O4/MoS2 (0.3)	Phenol (20)	49	0.126	0.171	[3]
SA-Cr/PN-g-C3N4 (0.2)	BPA (10)	163	0.0076	0.0023	[4]
Fe1-Nv/CN (0.5)	Ciprofloxacin (10)	9.9	0.0484	0.098	[5]
7% Cu-Fe2O3 (0.2)	Phenol (10)	10	0.0432	0.216	[6]
$CuFe_2O_4$	RhB	20	0.047	0.05875	[7]

(0.2)	(5)				
Ag_2/CFO_{Ovs} (0.1)	Phenol (50)	5	0.4448	44.48	[8]
CuO@NiAl-LDH (1.0)	MB (10)	100	0.0373	0.0034	[9]
Cu-N3 (0.3)	MB 10	30	0.0712	0.07911	[10]
$Fe_{0.8}Ce_{0.2}$-MIL-88B (0.1)	Tetracycline (50)	30	0.110	1.833	[11]
Ti-Mn_3O_4/Fe_3O_4 (1)	Tiamulin (5)	1	0.17	0.85	[12]
Fe2O3@FCNT-H (0.115)	MB (3.2)	50	0.0525	0.029	[13]
Cu/V_{550}-TCN (0.5)	Carbamazepine (10)	90	0.0490	0.011	[14]
FeOF (0.1)	p-nitrophenol (20)	10	0.362	7.24	[15]
FeP/Fe1-GO (0.15)	Tetracycline 12.7	100	0.097	0.082	[16]
Cu-C3N4 (1.0)	RhB (4.79)	29.41	1.64	0.267	[17]

$$K - value = \frac{k_{obs} \times C[pollutant]}{C[catalyst] \times C[H_2O_2]}$$

Reference

[1] C.H. Gu, S. Wang, A.Y. Zhang, C. Liu, J. Jiang, H.Q. Yu, Slow- release synthesis of Cu single-atom catalysts with the optimized geometric structure and density of state distribution for Fenton- like catalysis, Proc. Natl. Acad. Sci. U. S. A. 120(43) (2023) 12. https://doi.org/10.1073/pnas.2311585120.

[2] C.C. Ling, X.F. Liu, H. Li, X.B. Wang, H.Y. Gu, K. Wei, M.Q. Li, Y.B. Shi, H.J. Ben, G.M. Zhan, C. Liang, W.J. Shen, Y.L. Li, J.C. Zhao, L.Z. Zhang, Atomic-Layered Cu5 Nanoclusters on FeS2 with Dual Catalytic Sites for Efficient and Selective H2O2 Activation, Angewandte Chemie-International Edition 61(21) (2022) 8. https://doi.org/10.1002/anie.202200670.

[3] Q. Yan, C. Lian, K. Huang, L. Liang, H. Yu, P. Yin, J. Zhang, M. Xing, Constructing an acidic microenvironment by MoS2 in heterogeneous Fenton reaction for pollutant control, Angewandte Chemie International Edition 60(31) (2021) 17155-17163.

[4] F. Chen, X.L. Wu, C.Y. Shi, H.J. Lin, J.R. Chen, Y.P. Shi, S.B. Wang, X.G. Duan, Molecular Engineering toward Pyrrolic N-Rich M-N4 (M = Cr, Mn, Fe, Co, Cu) Single-Atom Sites for Enhanced Heterogeneous Fenton-Like Reaction, Advanced Functional Materials 31(13) (2021) 10. https://doi.org/10.1002/adfm.202007877.

[5] L.N. Su, P.F. Wang, X.L. Ma, J.H. Wang, S.H. Zhan, Regulating Local Electron Density of Iron Single Sites by Introducing Nitrogen Vacancies for Efficient Photo-Fenton Process, Angewandte Chemie-International Edition 60(39) (2021) 21261-21266. https://doi.org/10.1002/anie.202108937.

[6] H.Y. Zhan, R.R. Zhou, P.F. Wang, Q.X. Zhou, Selective hydroxyl generation for efficient pollutant degradation by electronic structure modulation at Fe sites, Proc. Natl. Acad. Sci. U. S. A. 120(26) (2023) 10. https://doi.org/10.1073/pnas.2305378120.

[7] L. Tian, Z.-J. Tang, L.-Y. Hao, T. Dai, J.-P. Zou, Z.-Q. Liu, Efficient Homolytic Cleavage of H2O2 on Hydroxyl-Enriched Spinel CuFe2O4 with Dual Lewis Acid Sites, Angewandte Chemie (2024)

e202401434.
[8] X.C. Ren, S.Y. Ding, R.H. Chen, Z.Y. Yang, M. Tian, N. Fu, Preparation of a novel Ag/CFOOVs composite catalyst and efficient degradation of phenol in a H2O2-based Fenton-like system, Journal of Alloys and Compounds 973 (2024) 14. https://doi.org/10.1016/j.jallcom.2023.172853.
[9] Y. Chen, H. Lian, H. Wang, J. Qin, X. Chen, Z. Lu, 3D flower-like CuO@ NiAl-LDH microspheres with enhanced removal affinity to organic dyes: mechanistic insights, DFT calculations and toxicity assessment, Journal of Materials Chemistry A 11(41) (2023) 22396-22408.
[10] F. Xu, C. Lai, M. Zhang, B. Li, L. Li, S. Liu, D. Ma, X. Zhou, H. Yan, X. Huo, High-loaded single-atom Cu-N3 sites catalyze hydrogen peroxide decomposition to selectively induce singlet oxygen production for wastewater purification, Applied Catalysis B: Environmental 339 (2023) 123075.
[11] M. Wu, Q.S. Wu, Y.K. Yang, Z.M. He, H.P. Yang, Regulating Lewis acidity and local electron density of iron-based metal organic frameworks via cerium doping for efficient photo-Fenton process, Journal of Colloid and Interface Science 630 (2023) 866-877. https://doi.org/10.1016/j.jcis.2022.10.122.
[12] X. Chen, W. Fu, Z. Yang, Y. Yang, Y. Li, H. Huang, X. Zhang, B. Pan, Enhanced H2O2 utilization efficiency in Fenton-like system for degradation of emerging contaminants: Oxygen vacancy-mediated activation of O2, Water Research 230 (2023) 119562.
[13] X. Xu, Y. Zhang, Y. Chen, C. Liu, W. Wang, J. Wang, H. Huang, J. Feng, Z. Li, Z. Zou, Revealing* OOH key intermediates and regulating H2O2 photoactivation by surface relaxation of Fenton-like catalysts, Proceedings of the National Academy of Sciences 119(36) (2022) e2205562119.
[14] J. Qiu, D. Wang, Y. Chang, Q. Feng, Z. Liu, M. Pang, D. Meng, Y. Feng, C. Fan, Anchoring single-atom Cu on tubular g-C3N4 with defect engineering for enhanced Fenton-like reactions to efficiently degrade carbamazepine: Performance and mechanism, Chemical Engineering Journal 479 (2024) 147841.
[15] D. Yu, L. Xu, K. Fu, X. Liu, S. Wang, M. Wu, W. Lu, C. Lv, J. Luo, Electronic structure modulation of iron sites with fluorine coordination enables ultra-effective H2O2 activation, Nature Communications 15(1) (2024) 2241.
[16] X.Y. Li, J.Y. Hu, Y.P. Deng, T. Li, Z.Q. Liu, Z. Wang, High stable photo-Fenton-like catalyst of FeP/Fe single atom-graphene oxide for long-term antibiotic tetracycline removal, Appl. Catal. B-Environ. Energy 324 (2023) 10. https://doi.org/10.1016/j.apcatb.2022.122243.
[17] J. Xu, X. Zheng, Z. Feng, Z. Lu, Z. Zhang, W. Huang, Y. Li, D. Vuckovic, Y. Li, S. Dai, Organic wastewater treatment by a single-atom catalyst and electrolytically produced H2O2, Nature sustainability 4(3) (2021) 233-241.